Appl. Phys. A 56, 219–225 (1993)

Applied Physics A Solids and Surfaces

Thermal Conductivity of C_{60} and C_{70} Crystals

N. H. Tea [1], R.-C. Yu [1,*], M. B. Salamon [1], D. C. Lorents [2], R. Malhotra [2], R. S. Ruoff [2]

[1] Department of Physics, University of Illinois at Urbana-Champaign, Urbana, IL 61801, USA
[2] SRI International, 333 Ravenswood Avenue, Menlo Park, CA 94025, USA

Received 8 September 1992/Accepted 12 November 1992

Abstract. We have performed thermal conductivity measurements on C_{60} and C_{70} crystals grown by sublimation. For single crystal C_{60}, the thermal conductivity κ is ~ 0.4 W/m K at room temperature and is nearly temperature independent down to 260 K. We observed a sharp orientiational phase transition at 260 K, indicated by a 25% jump in κ. Below 90 K, κ is time dependent, which manifests itself as a shoulder-like structure at ~ 85 K. The temperature and time dependence of κ below 260 K can be described by a simple model which accounts for the thermally activated hopping of C_{60} molecules between two nearly degenerate orientations, separated by an energy barrier of ~ 240 meV. It is found that solvents have a strong influence on the physical properties of C_{70} crystals. For solvent-free C_{70} crystal, κ is about constant above 300 K. There is a broad first-order phase transition in κ at 300 K with a 25% jump. We associate this transition with the aligning of the fivefold axes of the C_{70} molecules along the c-axis of the hexagonal lattice. Upon further cooling, κ increases and is time independent.

PACS: 66.70.+f, 64.70.Pf, 61.50.−f

Since the development of efficient techniques [1] for synthesizing C_{60} and C_{70}, tremendous research activity has been directed toward understanding the physical and chemical properties of the fullerenes and their derivatives. Recent progress has lead to the growth of large (mm-size) C_{60} crystals [2–3] that are free of solvents.

Experiments and theories have shown many remarkable features in the dynamics of solid C_{60}. X-ray [4–5], nuclear resonance [6], neutron scattering [7], sound velocity [8], dielectric constant [9], and thermal measurements [10–13] on C_{60} reveal an orientational ordering transition from a room temperature fcc structure to a sc structure at 260 K. Below this transition, the C_{60} molecules can still jump between nearly degenerate, inequivalent orientations, separated by energy barriers. Furthermore, the orientational order is time dependent, evident as a shoulder-like structure at about 85 K in the thermal conductivity [11]. Theoretical studies [14–15] show that the observed sc structure at low temperature can be understood if the Coulomb interactions between the electron-rich double bonds and the electron-poor single bonds are included in the Hamiltonian in addition to the usual Lennard-Jones potential.

The next higher stable fullerene is C_{70}, which has an elongated "rugbyball" shape. Its geometry suggests that there should be two possible phase transitions. The first corresponds to the locking of the fivefold axes of the C_{70} molecules along specific crystal directions and the second, to freezing of rotations about that axis. Vaughan et al. [16] reported two reproducible transitions at about 275 K and 335 K from differential scanning calorimetry (DSC) on solvent-free C_{70} powder which contained less than 20% hcp phase. They also found that the high temperature fcc phase is slightly lower in energy than the hcp phase but that the two phases coexist. However, for single crystals grown by sublimation starting from solvent-free C_{70} powder, there are two possible crystal structures – fcc and hcp. TEM studies [17] show that crystals with fcc structure have only one phase transition while crystals with hcp structure have more than one. However, mm-size C_{70} crystals have not been available until now. As a result, little is known about the dynamics of C_{70}.

In this paper, we describe the preparation of mm-size single crystals of both C_{60} and C_{70} by sublimation. We then report thermal conductivity measurements on solvent-free C_{60} and C_{70} crystals and on C_{70} crystals containing solvents. For C_{60}, we present a simple model that captures all the essential features in the thermal conductivity. This model takes into account the thermally activated hopping of the C_{60} molecules between two nearly degenerate orientations separated by a large energy barrier.

1 Sample Preparation

Fullerene-enriched soot was obtained by the arc-method [1]. C_{60} and C_{70} were extracted by high-performance liquid-column chromatography. The C_{60} powder obtained was

* *Permanent address*: Conductus, Inc., 969 W. Maude, Sunnyvale, CA 94086, USA

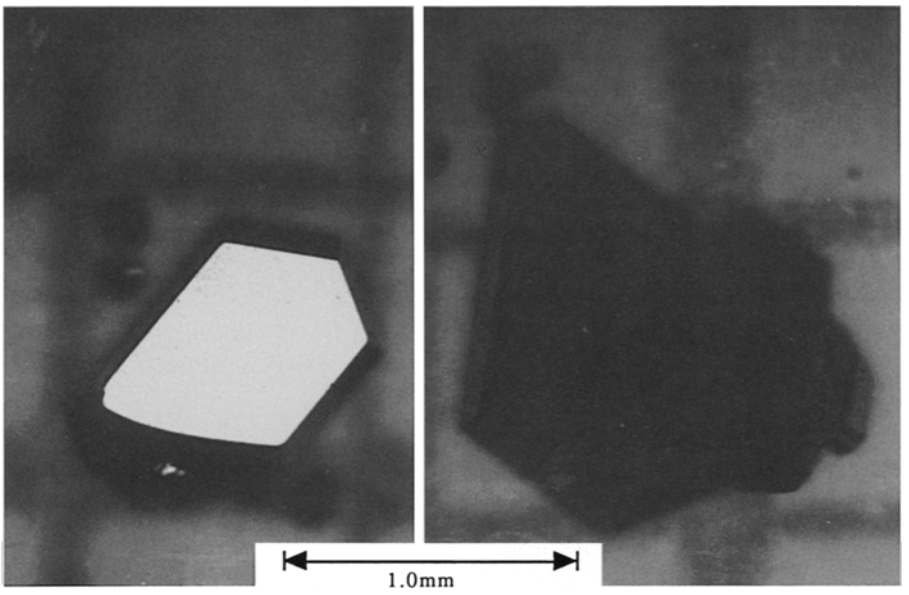

Fig. 1. Solvent-free C_{60} crystals grown by sublimation

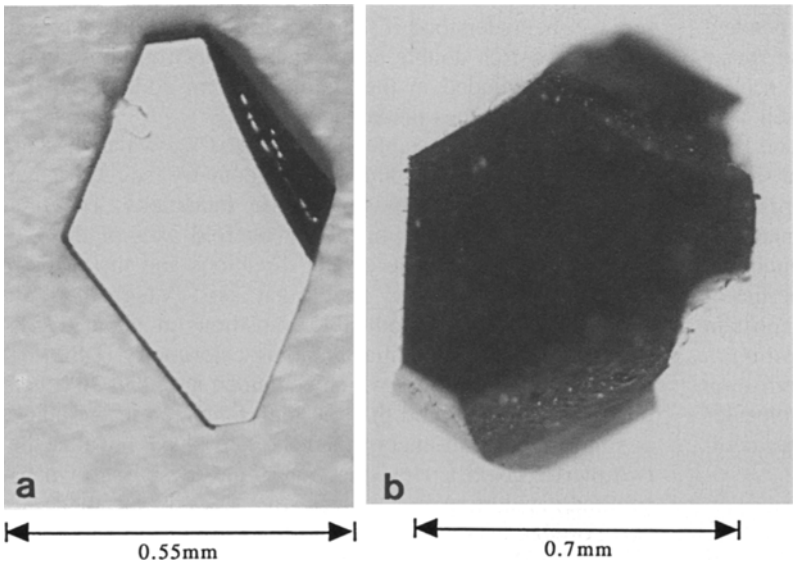

Fig. 2a, b. A C_{70} crystal containing solvents **a** and a solvent-free C_{70} crystal **b** grown by sublimation

99.5% pure. For C_{70}, repeated chromatography was necessary to obtain better than 99% purity. The purity of the C_{70} powder was determined by SALI (surface-analysis-by-laser-ionization) to be 99.85% pure. The C_{60} and C_{70} powders were dried under dynamic vacuum for 24 h at 200° C. This purification process yields highly crystalline C_{60}. About 30 mg of dry C_{60} powder was loaded in a quartz tube (4 mm ID and 6 mm OD) which was held at a pressure of 10^{-5} Torr for about 12 h after which the quartz tube was sealed under about 20 mTorr of ultra-high purity argon gas. The quartz tube was then placed in a furnace with a linear temperature gradient; the powder was held at 600° C and the cold end at 500° C. In about 100 h, mm-sized C_{60} crystals were obtained. Shown in Fig. 1 are C_{60} crystals about $0.5 \times 0.5 \times 1.0\,mm^3$ with a very flat shiny face. C_{60} crystals having a long rectangular shape, about 0.5 mm × 0.3 mm in cross-section ranging from 1 mm to 2 mm long, were also obtained.

C_{70} crystals prepared under the same conditions as C_{60} have shiny flat faces with dimensions of about $0.5 \times 0.4 \times 0.4\,mm^3$ as shown in Fig. 2a. These C_{70} crystals contain solvents and thermal conductivity results were not reproducible. To obtain better C_{70} powder, we follow the method used by Vaughan et al. [16]. Residual solvents were eliminated by subliming the C_{70} powder at 550° C in a dynamically pumped quartz tube. Solid C_{70} condensed only near the furnace exit and after 20 h, about 15 mg of C_{70} powder was collected. The dry C_{70} powder was then sealed under about 50 mTorr of argon gas in a quartz tube which was placed in a furnace with a linear temperature gradient. The powder was held at 600° C and the cold end at 500° C for 100 h. The temperatures of both ends were slowly cooled to 200° C and held at 200° C for two weeks. Crystals with dimension of about $0.5 \times 0.5 \times 0.9\,mm^3$ (see Fig. 2b) were selected for measurements.

X-ray diffraction at room temperature on C_{70} crystals containing solvents (from the same batch as the crystal in Fig. 2a) showed very faint blobs rather than sharp spots as expected for single crystals. Consequently, the lattice parameters cannot be determined. Raising the temperature to about 50° C showed no improvement indicating that the crystals have either a high density of defects, or coexistence of fcc and hcp phases. The room-temperature X-ray diffraction pattern of the crystal shown in Fig. 2b showed sharp spots that are very intense. The crystal has a hcp structure with $a = b = 10.18 \pm 0.01$ Å and $c = 18.72 \pm 0.01$ Å ($\alpha = \beta = 90°$ and $\gamma = 120°$. Verheijen et al. [17] found two hcp structures in their crystals with a hcp morphology at room temperature. Their lattice parameters are $a = b = 10.56$ Å and $c = 17.18$ Å and $a = b = 10.11$ Å and $c = 18.58$ Å, which agree well with our results.

2 Experimental

The thermal conductivity was measured by the static method. One end of the sample was attached to a block of quartz crystal and a miniature thin-film heater was attached on the other end of the sample. We also mounted a LakeShore silicon diode sensor on the quartz-crystal block. A pair of 12 µm Chromel-Constantan differential thermocouples was mounted on the sample with silver paste. The typical separation between the thermocouple junctions is about 0.2–0.3 mm. The temperature gradient was measured with the heater on and off after waiting for complete saturation of the thermal voltage (a typical delay of 30–60 s). The heat-pulse manipulation and data acquisition were controlled by a personal computer. The heat loss due to thermal conduction via the heater leads and thermocouples and to blackbody radiation is negligible.

3 Thermal Conductivity of C_{60} Single Crystals

Because C_{60} is a van der Waals-bonded molecular solid, its Debye temperature due to the intermolecular phonon modes is low $\theta_D \sim 70$ K [10]. For $T \gg \theta_D$, the specific heat due to propagating modes is constant. The sound velocity of a typical solid is approximately temperature independent, making the thermal conductivity κ an ideal probe of the phonon mean free path through the kinetic expression

$$\kappa = C v_s \lambda / 3 \tag{1}$$

where C is the specific heat, v_s is the sound velocity, and λ is the phonon mean free path. If the orientational disorder in C_{60} and C_{70} is one of the dominant scatterers of phonons, then measuring κ provides an excellent probe of the orientational order in solid C_{60} and C_{70}.

Shown in Fig. 3 is the temperature dependence of κ for a solvent-free single-crystal C_{60}. We find that $\kappa \sim 0.4$ W/m K at room temperature and is approximately temperature independent down to 260 K. At 260 K, κ takes a sharp jump from 0.4 to 0.5 W/m K with a transition width of $\sim$2 K. X-ray experiments [4–5] show that C_{60} undergoes a first-order orientational transition from a fcc structure to a sc structure at about the same temperature. Sound velocity

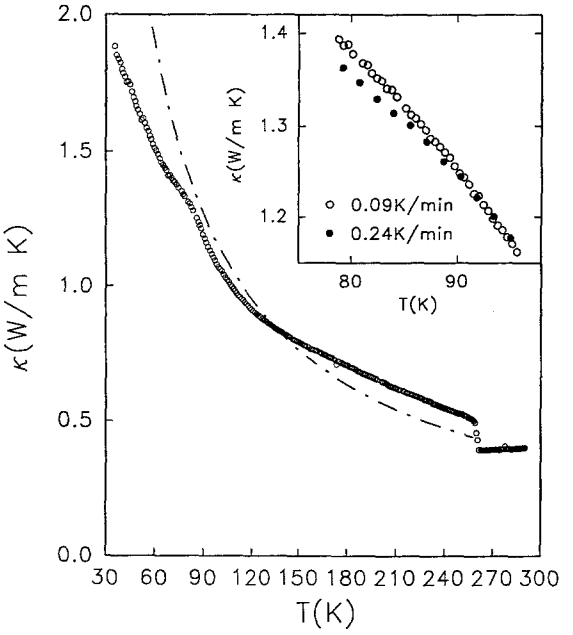

Fig. 3. The temperature dependence of the thermal conductivity of C_{60} single crystal. The *dot-dashed line* is an overlay of E/T for data below 260 K. Inset is a plot ot fhe thermal conductivity for two different cooling rates

measurements show only a 4% jump and the lattice constant changes only by $\sim$0.4%. Because the heat capacity due to intermolecular modes is constant at 260 K, the 25% jump in κ must be due to a sudden increase in the phonon mean free path. From NMR experiments [6], the motion of the C_{60} molecules was found to be fully dynamic above 260 K while neutron scattering experiments [18] characterized the motion of C_{60} as a continuous diffusive rotation. In other words, C_{60} molecules rotate essentially freely and isotropically (completely disordered) above 260 K. Below 260 K, the C_{60} molecules jump between discrete orientations separated by energy barriers. This suggests that orientational disorder in C_{60} causes strong phonon scattering which, in turn, limits the phonon mean free path. As a result, we expect that κ will have a very weak temperature dependence above 260 K, as indeed observed.

Below 260 K, the thermal conductivity increases with decreasing temperature and there is a reproducible shoulder-like structure at about 85 K. Further, the thermal conductivity was found to be time dependent. The cooling rate for the run shown in Fig. 3 is about 0.15 K/min. With decreasing cooling rate, we observed an enhanced κ at a characteristic temperature of about 90 K, as shown in the inset of Fig. 3. The run with a slower cooling rate, 0.09 K/min, results in a larger thermal conductivity than the run with a cooling rate of 0.24 K/min.

To explore this time-dependent property, we measured κ at several temperatures in the vicinity of 90 K as follows. First, the temperature was held at 130 K for a few minutes, followed by rapid cooling to the target temperature in about 1800 s. When the temperature reached the target temperature, we took data continuously until κ saturated. The target temperature was stabilized to better than 1%. Shown in Fig. 4 is the time dependence of κ at three different temperatures. The thermal conductivity increases with time and then saturates with a different relaxation time at each temperature.

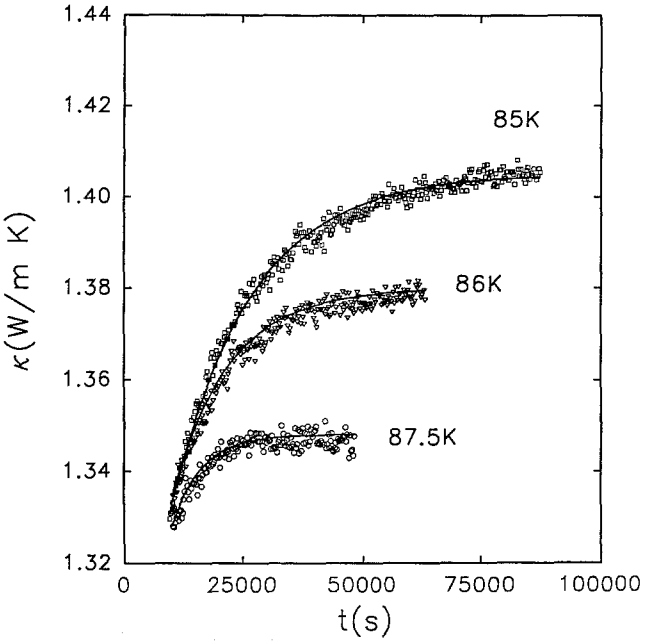

Fig. 4. The time dependence of the thermal conductivity of C_{60} at 87.5, 86, and 85 K (from [11]). The *solid lines* are plots of (6) using κ_f and $\ln C$ obtained from Fig. 6

4 Phenomenological Model

For insulators at high temperature, Umklapp processes dominate and the temperature dependence of the thermal conductivity κ_u goes as $1/T$. Shown in Fig. 3 is an overlay of $\kappa_u = E/T$, where E is an adjustable parameter for data below 260 K. Clearly, there are discrepancies between the experimental data and κ_u, especially for $T < 90$ K and $T > 150$ K. As shown below, this substantial deviation from 1/T-behavior arises mostly from the measurement time scale imposed by the experiments.

In order to understand the unusual shoulder-like structure at about 85 K, we must take into account not only the temperature dependence of κ but also its time dependence. We first write $\lambda = v_s\tau$, where $\tau^{-1} = \sum_{i=1}^{n} \tau_i^{-1}$ is the total scattering rate, and i denotes the various scattering mechanisms. At high temperature, phonon-phonon scattering via Umklapp processes play an important role in determining the thermal conductivity. This scattering rate is proportional to temperature, $\tau_u^{-1} \propto T$. Because the phonon scattering rate depends on the orientational disorder, the thermal conductivity will also be time dependent. To account for this time dependence, we introduce the orientational disorder scattering rate τ_{od}^{-1}, which is proportional to the occupation probability of misorientations $n_d(T,t)$. For simplicity, we assume that the temperature dependence of τ_{od}^{-1} is entirely due to $n_d(T,t)$. Then the total scattering rate is given by

$$\tau = \frac{1}{\tau_{od}^{-1} + \tau_u^{-1}} . \tag{2}$$

The thermal conductivity $\kappa \propto \tau$ and we can write it as

$$\kappa = \frac{A}{n_d(T,t) + BT} . \tag{3}$$

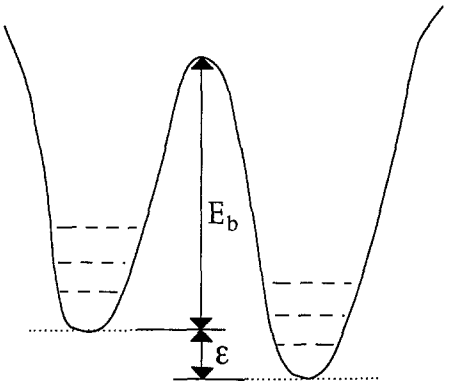

Fig. 5. Sketch of the double well potential for the two nearly degenerate orientations, $E_b \gg \varepsilon$

To proceed, we need to know $n_d(T,t)$. A recent calculation by Lu et al [14] shows that below about 270 K, there exist many nearly degenerate orientations separated by potential barriers of order ~300 meV. For simplicity, we assume two such orientations separated by an energy barrier E_b, as shown in Fig. 5. The energy difference between these orientations is ε, where $E_b \gg \varepsilon$. If ν is the average librational frequency of the C_{60} molecules and the interactions between C_{60} molecules are neglected, then the rate for a C_{60} molecule to thermally jump from one orientation to the other is

$$t_r^{-1} = \nu e^{-E_b/k_B T} . \tag{4}$$

The occupation probability of misorientations is given by

$$n_d(T,t) = [n_d(T,0) - n_d(T,\infty)]e^{-t/t_r} + n_d(T,\infty) \tag{5}$$

and $n_d(T,\infty) = 1/[1 + \exp(\varepsilon/k_B T)]$ is the thermal equilibrium population. By combining (2) and (5), the thermal conductivity can be written as

$$\kappa = \frac{1}{C\exp(-t/t_r) + \kappa_f^{-1}} , \tag{6}$$

where $C = [n_d(T,0) - n_d(T,\infty)]/A$ and κ_f is the thermal conductivity as $t \to \infty$ given by

$$\kappa_f = \frac{A}{n_d(T,\infty) + BT} . \tag{7}$$

Taking the logarithm of (6) puts the thermal conductivity in a useful form for analysing the data plotted in Fig. 4. The resulting equation is

$$\ln(\kappa^{-1} - \kappa_f^{-1}) = \ln C - t/t_r . \tag{8}$$

In Fig. 4, we take the saturated values of κ as κ_f and plot the data in the form of (8) in Fig. 6. The data conform to a straight line very well. We extract the relaxation time t_r at three different temperatures by a least-squares fit. In the inset, we plot $\ln t_r$ versus $1/T$ and a straight line can be drawn through the data. From a least-squares fit, we obtained an energy barrier $E_b = 240 \pm 30$ meV from the slope and $\nu = 10^{12\pm2}$ from the intercept.

In order to fit the temperature-dependent thermal conductivity, we must account for the finite time spent at each temperature, especially for data points below about 90 K.

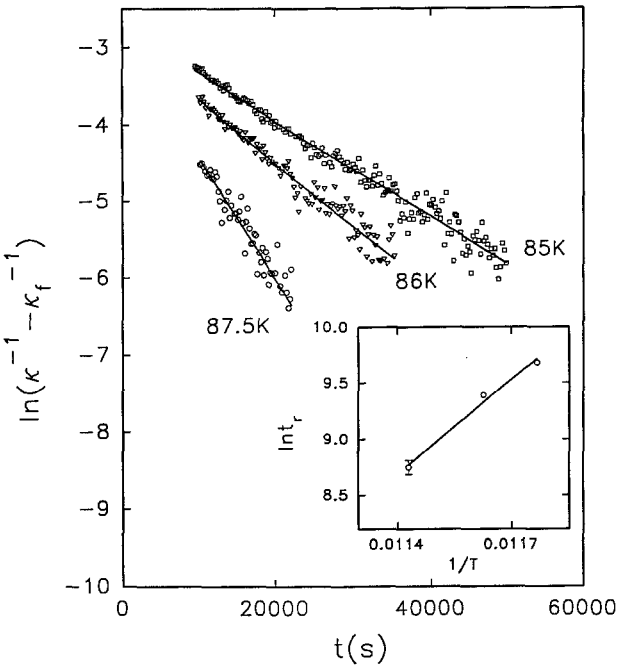

Fig. 6. The time dependence of κ plotted in the form of (8) at 87.5, 86, and 85 K (from [11]). Inset is a $\ln t_r$ vs $1/T$ plot. The *solid lines* are linear least-squares fits

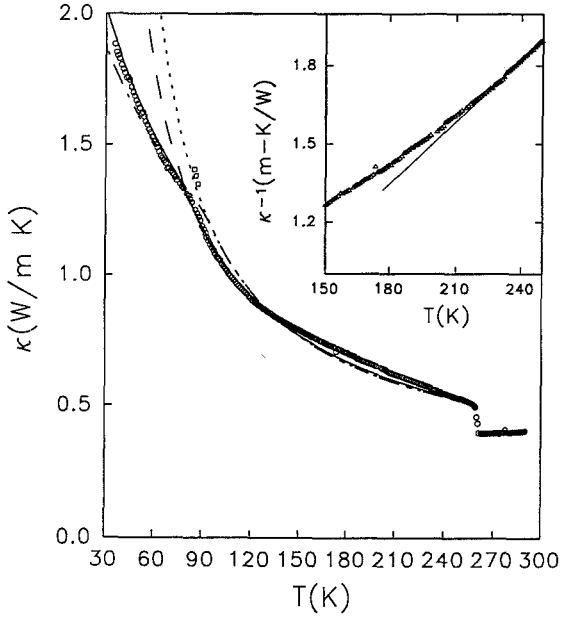

Fig. 7. The temperature dependence of the thermal conductivity of C_{60} single crystal. Open squares are the saturated thermal conductivity data from Fig. 4. The *solid line* is a least-squares fit for the data below 150 K. The *dashed line* is a plot of (7) using the least-squares-fit parameters. The *dot-dashed line* is the curve from our previous analysis [11] and the dotted line is the equilibrium thermal conductivity from [11]. Inset is a κ^{-1} vs T plot. The *straight line* is a guide for the eye

The typical time spent at each data point is about 300 s. We take $n_{d,i}(T_i, t_i)$ as $n_{d,i-1}(T_{i-1}, t_{i-1})$, where t_{i-1} is the time taken at point $i-1$ and we obtained the following relation

$$n_{d,i}(T_i, t_i) = [n_{d,i-1}(T_{i-1}, t_{i-1}) - n_d(T_i, \infty)] \times e^{-t_i/t_r(T_i)} + n_d(T_i, \infty) \quad (9)$$

The adjustable parameters are A, B, ε, ν and E_b. The values obtained from the best representation by (6) in our earlier analysis [11] are $A = 0.42$ W/m K, $B = 0.0018\,K^{-1}$, $\varepsilon = 12$ meV, $E_b = 271$ meV, and $\nu = 3 \times 10^9\,s^{-1}$. These parameters together with t_r and κ_f obtained from Figs. 4 and 6 are presented in Table 1. These parameters were chosen so that κ_f passes through the time-dependent data. As a result of this compromise, the curve only crosses the temperature-dependent data at several points.

Another way to extract E_b and ν is to carry out a least-squares fit of the temperature-dependent thermal conductivity to (6). The inset of Fig. 7 shows a plot of κ^{-1} versus T. Clearly, the thermal conductivity does not follow the $1/T$-form, so we carried out a least-squares fit to (6) only for the data below 150 K. The best fit was obtained with $A = 0.643$ W/m K, $B = 0.00332\,K^{-1}$, $\varepsilon = 8.7$ meV, $E_b = 240.5$ meV, and $\nu = 6.3 \times 10^9\,s^{-1}$. These parameters are also presented in Table 1. $E_b = 240.5$ meV obtained from the least-squares fit to our thermal conductivity data is comparable to $E_b = 240$–248 meV from sound-velocity measurements [8], $E_b = 250$ meV from NMR experiments [6], $E_b = 270$ meV from dielectric constant measurements [9], and $E_b = 230$ meV from heat capacity measurements [13]. Recently, Matsuo et al. [13] reported temperature and time dependence of the heat capacity of solvent-free C_{60} powder. Their time-dependent measurements are similar to the method used in our thermal conductivity experiments. Our ν of $6.3 \times 10^9\,s^{-1}$ agrees very well with their $\nu = 2.5 \times 10^{10\pm1}\,s^{-1}$.

In Fig. 7, we show a plot of κ (dot-dashed line) and κ_f (dotted line), which represents the thermal equilibrium value of the thermal conductivity, from [11]. Also shown in Fig. 7 are κ (solid line) and κ_f (dashed line) generated from the least-squares-fit parameters. Both κ's reproduce well the temperature dependence of the thermal conductivity data including the shoulder-like structure at 85 K. As a result of our choice of parameters [11], κ_f (dotted line) also goes through the time-dependent data. However, κ_f (dashed line) calculated from the least-squares-fit parameters does not go through the saturated κ_f obtained from time-dependent measurements. This discrepancy is not surprising, given the crudeness of our model. Theoretical model [14] predicts a variety of energy barriers and consequently, a range of relaxation times. Evidently, fits to the short-time behavior represented in Fig. 7 tend to overestimate the ultimate long-time limit of the disorder probed by the data of Fig. 4. Also

Table 1. The fitting parameters

T [K]	t_r [10^4 s]	κ_f [W/m K]	E_b [meV]	ε [meV]	ν [s^{-1}]	A [W/m K]	B [K^{-1}]
87.5	0.63 ± 0.04	1.348					
86.0	1.20 ± 0.2	1.380					
85.0	1.60 ± 0.2	1.405					
Parameters from [11]			271.0	12.3	3.0×10^9	0.420	0.00180
Least-squares-fit parameters			240.5	8.70	6.3×10^9	0.643	0.00332

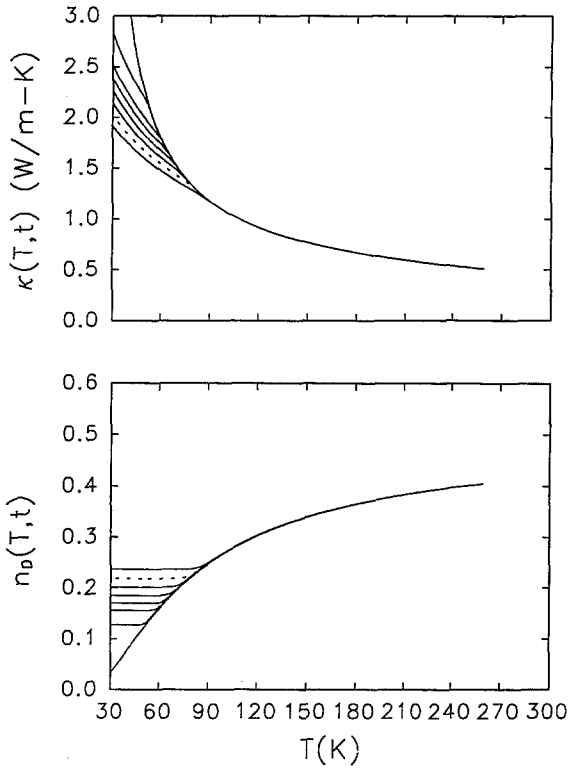

Fig. 8. Plots of the thermal conductivity and occupation probability of misorientations from the least-squares-fit parameters with various wait times between data points. From bottom to the top $\kappa(T,t)$-curves, the wait time between data points is, respectively, 15 s, 300 s, 6×10^3 s, 1.2×10^5 s, 2.4×10^6 s, 4.8×10^7 s, 3.8×10^{10} s, ∞. The *dotted line* represents our experimental time scale

we assume in our model that $n_{\mathrm{d},i}(T_i, t_i) = n_{\mathrm{d},i-1}(T_{i-1}, t_{i-1})$ which does not account for the variation in n_{d} between data points. However, the qualitative picture described here should remain valid. This simple model shows that the shoulder-like structure at 85 K is due to the measurement time scale imposed by the experiments.

Our simple model considers only two nearly degenerate orientations and does not include other scattering mechanisms such as defect scattering, four-phonon scattering, phonon-libron scattering, etc. The model also assumes that the sound velocity and the heat capacity are temperature independent and neglects possible phonon scattering from the intramolecular modes. Solid C_{60} has many nearly degenerate orientations at low temperature and a more complete calculation should take these into account. However, the qualitative description of the glassy behavior is expected to remain unchanged.

Shown in Fig. 8 are plots of the calculated κ and the occupation probability of misorientations $n_{\mathrm{d}}(T,t)$, using the least-squares-fit parameters with various wait times between data points for the double-well model. Clearly for $T < 90$ K, the values of the thermal conductivity approach the equilibrium values as the time taken between data points approaches infinity. For $T > 90$ K, the calculated κ is time independent. The occupation probably for temperatures below the shoulder-like structure is essentially frozen due to the long relaxation time t_{r} required for the molecules to reorient. This means that orientational disorder is always present at low temperature unless the experimental time scale is infinitely long. Our experimental time scale corresponds to a frozen value of about 22% in the occupation probability shown as the dotted line in Fig. 8. Indeed, a recent neutron scattering experiment by David et al. [7] found that about 18% static orientational disorder persists down to 10 K. Our earlier analysis [11] showed a frozen-in disorder of about 17%. A theoretical calculation by Lu et al. [14] showed that, because many local energy maxima exist at low temperature, there is a glassy transition between 90 K and 130 K depending on the experimental time scale. Below this transition, the disorder becomes frozen.

5 Thermal Conductivity of C_{70}

Solid C_{70} has a "rugbyball" shape; we naively expect that there must be at least two phase transitions. Further, its elongated shape should inhibit rotations; thus, its transition temperature should be higher than C_{60}. Because its shape makes it similar to the classic $(KBr)_{1-x}(KCN)_x$ orientational glass and C_{60} was shown to be orientationally disordered below 90 K, we wish to explore these possibilities in solid C_{70}.

Shown in Fig. 9 is the temperature dependence of the thermal conductivity of C_{70} crystals containing solvents. The thermal conductivity varies from run to run and was highly non-reproducible. Further, there is an unusual peak in the thermal conductivity on warming. Unlike solvent-free C_{60} crystals, the thermal conductivity decreases with decreasing temperature. This type of temperature dependence is similar to amorphous solids and conventional glasses such as vitreous silica where the phonon mean free path increases slowly with decreasing temperature and κ follows approximately the heat capacity. If the pure C_{60} extract was not dried at 200° C for 24 h, its high resolution ac heat capacity [19] showed an orientational phase transition at 220 K rather than at 260 K for solvent-free C_{60}. In a recent paper by Atake et al. [20], solvents were found to have a strong influence on the orientational phase transition in solid C_{60}.

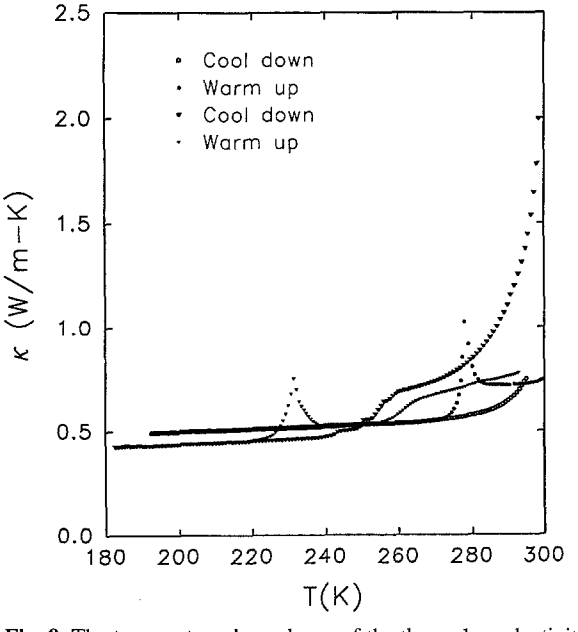

Fig. 9. The temperature dependence of the thermal conductivity of C_{70} crystals containing solvents

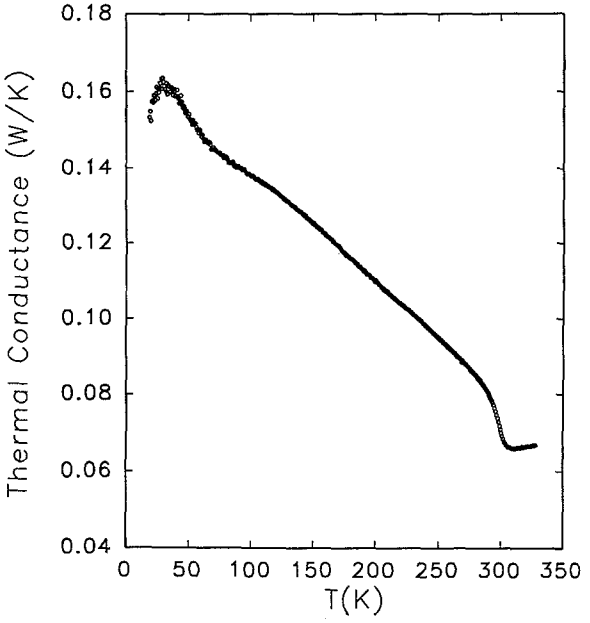

Fig. 10. The temperature dependence of the thermal conductance of a solvent-free C_{70} crystal

Shown in Fig. 10 is the temperature dependence of the thermal conductance of solvent-free C_{70} crystals. Because the shape of the C_{70} crystals is quite irregular, an accurate calculation of the thermal conductivity is not possible. The thermal conductance is ~ 0.068 W/K above about 300 K. At about 300 K, there is a 25% jump in the thermal conductance with a broad transition width of ~ 15 K. The size of this jump is the same as in C_{60} crystals. Below this transition, the thermal conductance increases with decreasing temperature, analogous to the thermal conductivity of solvent-free C_{60} crystals. The thermal conductance reaches a maximum at about 25 K and then decreases with decreasing temperature.

Vaughan et al. [16] have performed DSC measurements on solvent-free C_{70} powder and found two reproducible phase transitions at about 275 K and 335 K. They also found coexistence of fcc and hcp phases in their C_{70} powder but that the hcp phase could be reduced by annealing. A recent TEM diffraction experiment by Verheijen et al. on solvent-free C_{70} crystals found that, for C_{70} crystals with an fcc structure, there is a single phase transition while for C_{70} crystals with a hcp structure, there are several transitions. They suggest that the crystals with hcp structure undergo two transitions: alignment of the fivefold axes of the C_{70} molecules with the c-axis of the hexagonal lattice somewhat above room temperature and freezing of rotations about the fivefold axis near the ice point. We attribute the jump at about 300 K in our thermal conductance with the alignment of the fivefold axes of the C_{70} molecules along the c-axis of the hexagonal lattice. We have also performed high-resolution ac heat capacity measurements on these solvent-free C_{70} crystals and the results together with detailed measurements of the thermal conductance will be reported elsewhere. Unlike C_{60} crystals which become an orientational glass at ~ 90 K, the thermal conductance of C_{70} crystals shows no time dependence from 370 K down to 15 K.

In summary, we have measured the thermal conductivity of C_{60} and C_{70} crystals that are free of solvents and C_{70} crystals that contain solvents. At 260 K, C_{60} crystals undergo a first-order phase transition from a fcc structure to a sc structure. Below 90 K, the thermal conductivity of C_{60} is time dependent which is interpreted as freezing of the orientational disorder. A simple model is developed to explain the temperature and time dependence of the thermal conductivity of C_{60}. The temperature dependence of the thermal conductivity of C_{70} crystals containing solvents behaves like amorphous solids and is non-reproducible. Solvent-free C_{70} crystals undergo a first-order phase transition at about 300 K. We identify this transition as the alignment of the fivefold axes of the C_{70} molecules along the c-axis of the hexagonal lattice.

Acknowledgements. We would like to thank J.P. Lu for stimulating discussions and for encouragements during the early phase of this project and Scott Wilson for the X-ray analysis. One of us (NHT) also like to thank Gavin Vaughan, Ken Ghiron, Jing Shi, Brenda Everitt, and Bob Beach for helpful discussions and K. O'Hara for use of his fitting program. This work has been supported by National Science Foundation Grant No. DMR 89-20538 through the Illinois Materials Research Laboratory.

References

1. W. Krätschmer, D. Lamb, K. Fostiropoulos, D.R. Huffman: Science **347**, 354 (1990)
2. X.-D. Xiang, J.G. Hou, G. Briceno, W.A. Vareka, R. Mostovoy, A. Zettl, V.H. Crespi, M.L. Cohen: Science **256**, 1190 (1992)
3. J. Li, S. Komiya, T. Tamura, C. Nagasaki, J. Kihara, K. Kishio, K. Kitazawa: Physica C **195**, 205 (1992)
4. P.A. Heiney, J.E. Fischer, A.R. McGhie, W.J. Romanow, A.M. Denenstein, J.P. McCauley Jr., A.B. Smith III, D.E. Cox: Phys. Rev. Lett. **66**, 2911 (1991)
5. M. Moret, P.A. Albouy, V. Agafonov, R. Ceolin, D. Andre, A. Dworkin, H. Szwarc, C. Fabre, A. Rassat, A. Zahab, P. Bernier: J. Phys. 1 (France) **2**, 511 (1992)
6. R. Tycko, G. Dabbagh, R.M. Fleming, R.C. Haddon, A.V. Makhija, S.M. Zahurak: Phys. Rev. Lett. **67**, 1886 (1991)
7. W.I.F. David, R.M. Ibberson, T.J.S. Dennis, J.P. Hare, K. Prassides: Europhys. Lett. **18**, 219 (1992)
8. X.D. Shi, A.R. Kortan, J.M. Williams, A.M. Kini, B.M. Savall, P.M. Chaikin: Phys. Rev. Lett. **68**, 827 (1992(
9. G.B. Alers, B. Golding, A.R. Kortan, R.C. Haddon, F.A. Theil: Science **257**, 511 (1992)
10. T. Atake, T. Tanaka, H. Kawaji, K. Kikuchi, K. Saito, S. Suzuki, I. Ikemoto, Y. Achiba: Physica C **185**, 427 (1991)
11. R.C. Yu, N.H. Tea, M.B. Salamon, D. Lorents, R. Malhotra: Phys. Rev. Lett. **68**, 2050 (1992)
12. M. Chung, Y. Wang, J.W. Brill, X.-D. Xiang, R. Mostovoy, J.G. Hou, A. Zettl: Phys. Rev. B **45**, 13831 (1992)
13. T. Matsuo, H. Suga, W.I.F. David, R.M. Ibberson, P. Bernier, A., Zahab, C. Fabre, A. Rassat, A. Dworkin: Solid State Commun. **83**, 711 (1992)
14. J.P. Lu, X.-P. Li, R.M. Martin: Phys. Rev. Lett. **68**, 1551 (1992)
15. M. Sprik, A. Cheng, M.L. Klein: J. Phys. Chem. **96**, 2027 (1992)
16. G.B.M. Vaughan, P.A. Heiney, J.E. Fischer, D.E. Luzzi, D.A. Ricketts-Foot, A.R. McGhie, Y.-W. Hui, A.L. Smith, D.E. Cox, W.J. Romanow, B.H. Allen, N. Coustel, J.P. McCauley Jr., A.B. Smith III: Science **254**, 1350 (1991)
17. M.A. Verheijen, H. Meekes, G. Meijer, P. Bennema, J.L. deBoer, S. van Smaalen, G. van Tendeloo, S. Amelinckx, S. Muto, J. Van Landuyt: Chem. Phys. (in press, 1992)
18. D.A. Neumann, J.R.D. Copley, R.L. Cappelleti, W.A. Kamitakahara, R.M. Lindstrom, K.M. Creegan, D.M. Cox, W.J. Ramanow, N. Coustel, J.P. McCauley Jr., N.C. Maliszewskyj, J.E. Fischer, A.B. Smith III: Phys. Rev. Lett. **67**, 3808 (1991)
19. K. Ghiron, N. Tea, M.B. Salamon, S. Keofod, J. Shapley: Unpublished
20. T. Atake, T. Tanaka, H. Kawaji, K. Kikuchi, K. Saito, S. Suzuki, Y. Achiba, I. Ikemoto: Chem. Phys. Lett. **196**, 321 (1992)